NUCL SCI TECH (2018) 29:141
https://doi.org/10.1007/s41365-018-0488-8

Numerical study of the dynamic characteristics of a single-layer graphite core in a thorium molten salt reactor

Yang Zhong[1,2] · Xiong Yang[1,2] · Dong Ding[1,2] · Yang Zou[1] · D. K. L. Tsang[1]

Received: 4 January 2018 / Revised: 10 April 2018 / Accepted: 11 April 2018 / Published online: 29 August 2018

Abstract A reactor core in a thorium molten salt reactor uses graphite as a moderator and reflector. The graphite core is a multi-layered arrangement of graphite bricks that are loosely connected to each other using a system of keys and dowels. Consequently, the graphite core is a type of discrete stack structure with highly nonlinear dynamic behavior. Hence, it is important to investigate the dynamic characteristics of the graphite core. In this study, a three-dimensional single-layer graphite core model, which is a part of the thorium molten salt reactor side reflector structure, was analyzed using the explicit method in ABAQUS 2016 to study the core dynamic behavior when subjected to different excitations. The design parameters, such as the diameter of the dowel, the gap between key and keyway and the bypass flow gap between two adjacent bricks, were also considered in this model. To reduce excessive demands on available computational resources considering the effect of molten salt, the spring–dashpot model was applied to model the interaction forces between the molten salt and graphite bricks. Numerical simulation results show that the effect of molten salt is a reduction in the peak maximal principal stress, and a larger gap between two bricks is beneficial to maintain the integrity of the graphite core under earthquake loading. The results obtained by the simulation can be used as a reference for future designs of a molten salt graphite core.

Keywords Graphite core · Dynamic behavior · ABAQUS

This work was supported by the "Hundred Talent Program" of the Chinese Academy of Sciences, the Ministry of Human Resources and Social Security (No. Y419016031), and the Strategic Priority Research Program of Chinese Academy of Science (No. XDA02040100).

✉ D. K. L. Tsang
derektsang@sinap.ac.cn

1 Shanghai Institute of Applied Physics, Chinese Academy of Sciences, Shanghai 201800, China

2 University of Chinese Academy of Sciences, Beijing 100049, China

1 Introduction

The Chinese Academy of Sciences (CAS) has launched a strategic priority research project to utilize thorium energy via the development of a thorium molten salt reactor (TMSR) to secure a long-term nuclear fuel supply by diversifying the sources of nuclear fuel [1, 2]. The reactor core in a TMSR contains graphite components used as moderator and reflector. The graphite core is a multi-layered arrangement of graphite bricks that are loosely connected to each other using a system of keys and dowels. The graphite core is a type of discrete stack structure with highly nonlinear dynamic behavior and its behave completely differently in terms of dynamic response compared to a welded structure or bolted structure when subjected to seismic loading [3, 4]. Hence, it is important to investigate the dynamic characteristic of the TMSR graphite core assembly.

According to Institute of Electrical and Electronics Engineers Standard 344 [5], during an earthquake the reactor core requires structural integrity to be maintained and safe shutdown of the reactor. The core is required to withstand two types of earthquakes, namely an operating basis earthquake (OBE) and a safe shutdown earthquake (SSE). An OBE is an earthquake that could reasonably be expected to occur at the site during the operating life of the reactor and the reactor is designed to remain functional. An SSE is an earthquake that is based upon an evaluation of the maximal earthquake potential considering the regional and local geology and seismology and the specific characteristics of the local subsurface material. An SSE produces a maximal vibratory ground motion for which the capability to shut down the reactor and maintain it in a safe shutdown condition is required. The fundamental safety requirements of the graphite core are to allow free movement of control rods and to direct the flow of coolant to ensure adequate cooling of the fuel and the core structure, both in normal and fault/hazard conditions. Consequently, a safety analysis demonstrating the tolerability of the core safety functions to geometrical changes and earthquakes is required.

An understanding of the dynamic response of the graphite core and the internal stress of individual graphite components under normal operation and transient conditions is essential in assessing core geometry; structure integrity; inspection strategy; and, consequently, core safety. A numerical method plays a principal role in the dynamic analysis of the graphite core. One major advantage of this method is that it can provide detailed displacement and stress distribution information for individual components. It also can allow for more complex analysis and inaccessible experimental conditions.

Reactors including a gas-cooled reactor, advanced gas-cooled reactor (AGR), high-temperature gas-cooled reactor (HTGR) and molten salt reactor have a graphite core. The dynamic analysis of a graphite core using a numerical method has occurred quite often during the past decades. For an HTGR, Merson and Bennett developed a small number of degrees-of-freedom computer program to study the seismic response of an HTGR core [6]. Ikushima and Honma contrived a simplified model for HTGR core seismic analysis to reduce the considerable computational cost. In this code, one degree-of-freedom mass with nonlinear column characteristics has been used instead of a stacked column [7]. Considering the pebble-bed HTGR has various graphite shapes, a generalized three-dimensional (3D) model with the associated computer code was developed to treat these interconnected graphite bricks with arbitrary shapes by Zeng and Wang [8]. In this model, each brick is treated as a rigid body with six degrees-of-freedom: three translational displacements and three rotations around the brick center of gravity. A nonlinear spring dashpot model has been applied to model the collision between adjacent bricks and the interaction forces through the key systems. Tsuji and Ohashi [9] developed a vertical two-dimensional analytical model using multi-purpose commercial finite element method (FEM) code, which considers the multiple impacts and friction between block interfaces and rocking motion in contact with dowel pins of the HTGR core using contact elements. For an accurate prediction response of an AGR core to an earthquake, Ahmed et al. [10] proposed an analytical method with several hundred thousand degrees of freedom for an AGR reactor. The graphite bricks which comprise the core were idealized as rigid masses, whilst the contact spring elements were used to represent the load transmissions or impacts that could occur between the bricks. The graphite core of the AGR core has been seismically qualified using the non-linear computer program AGRCOR [11, 12]. Graphite bricks have been treated as rigid bodies and each brick has three degrees of freedom: two translational displacements and one rotation.

However, few works have addressed the dynamic behavior of the graphite core in a TMSR. The difference between a TMSR and other types of graphite-moderated reactors is the existence of molten salt, which is a vital factor influencing the dynamic response of the graphite core, because the mass density of molten salt is much higher than that of a gas coolant. In addition, the aforementioned literature used a rigid body and limited dimensions in numerical analysis. For a better understanding of the dynamic response of graphite cores and the internal stress of individual core components in a TMSR, graphite bricks cannot be treated as a rigid body and the model should be three-dimensional with full stress analysis. In this study, analysis was conducted using the FEM program ABAQUS 2016. A single layer of graphite core was built. Each brick was treated as a deformable body. Because the design of the TMSR graphite core brick is different from that of the other graphite-moderated reactors, several design parameters such as the diameter of the dowel, the gap between key and keyway and bypass flow gaps were also considered in this model to investigate how these parameters influence the dynamic responses and stresses within the graphite bricks.

2 Numerical study

2.1 Explicit dynamic analysis

The equation of equilibrium governing the dynamic response of a system in the FEM program at time t_n is generally expressed as follows:

$$\mathbf{M}\ddot{\mathbf{u}}_n + \mathbf{C}\ddot{\mathbf{u}}_n + \mathbf{F}_n^{\text{int}}(\mathbf{u}_n) = \mathbf{R}_n, \tag{1}$$

where $\mathbf{M}$ is the mass matrix and $\mathbf{C}$ is the damping matrix; $\mathbf{R}_n$ is the vector of the externally applied loads; $\mathbf{F}_n^{\text{int}}$ is the internal force vector; and $\ddot{\mathbf{u}}_n$, $\dot{\mathbf{u}}_n$, $\mathbf{u}_n$ are the acceleration, velocity and displacement vectors, respectively.

Equation (1) is integrated by an explicit central difference integration rule and can be written as follows:

$$\ddot{\mathbf{u}}_n = \mathbf{M}^{-1}\left[\mathbf{R}_n - \mathbf{C}\dot{\mathbf{u}}_n - \mathbf{F}_n^{\mathrm{int}}(\mathbf{u}_n)\right]. \tag{2}$$

Velocities and displacements are updated in each time step as follows:

$$\dot{\mathbf{u}}_{n+1/2} = \dot{\mathbf{u}}_{n-1/2} + \Delta t_n \ddot{\mathbf{u}}_n, \tag{3}$$

$$\mathbf{u}_{n+1} = \mathbf{u}_n + \Delta t_{n+1/2}\dot{\mathbf{u}}_{n+1/2}, \tag{4}$$

where $\Delta t_n = (\Delta t_n + \Delta t_{n+1})/2$.

The explicit integration scheme has a very important advantage in that it improves the computational efficiency by using a diagonal mass matrix because the inversion of the mass matrix used in Eq. (2) is trivial. Among the disadvantages of the explicit integration procedure is the stability of the numerical integration. To achieve stability, the calculation time step size must be smaller than the critical time step Δt_{cr}, which is determined by the character length of the elements and their material properties. For a finite element mesh of constant strain and rate independent materials, the critical time step can be calculated as follows:

$$\Delta t_{\mathrm{cr}} \le \min_{\mathrm{e}}(l_{\mathrm{e}}/c_{\mathrm{e}}), \tag{5}$$

where l_{e} is the character length of the element and c_{e} is the wave speed in the element [13].

2.2 Fluid–structure coupling method

In TMSR, all the graphite components with narrow gaps between them are immersed in molten salt. It is difficult to construct the finite element model of the totally assembled reactor internals with molten salt using the coupled Eulerian–Lagrangian method because of the complex multibody interaction, boundary conditions and limitation on computational time and physical memory of the computer. The effects of fluid on the brick can be regarded as the stiffness k and damping c of the spring element [14]. Spring-like elastic behavior and dashpot-like (damping) behavior are used in the model to consider fluid–structure interaction (FSI). The graphite brick is subjected to sinusoidal harmonic $P(t)$. The effect of the fluid–structure interaction between the two bricks can be simplified as an added mass, added damping and added stiffness coefficient as shown in Fig. 1.

In this model, the graphite brick is supported by six parallel springs. If the effect of the molten salt is negligible, the free vibration equation of the brick is as follows [15, 16]:

$$m\ddot{y} + Ky = 0, \tag{6}$$

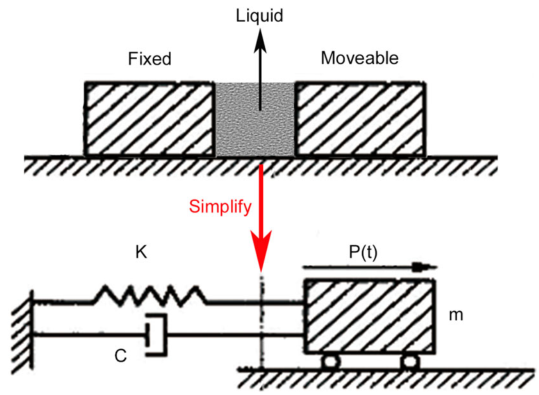

Fig. 1 Simplification of brick vibration in the TMSR

where m and K are the mass of the brick and the stiffness of the spring, respectively; y is the displacement of the brick; and $\ddot{y}$ is the acceleration of the brick. When the brick vibrates in the fluid, the added damping and resistance force are produced. The vibration equation of the brick in the fluid is written as follows:

$$(m + m_{\mathrm{ad}})\ddot{y} + C_{\mathrm{ad}}\dot{y} + (K + k_{\mathrm{ad}})y = 0, \tag{7}$$

where C_{ad} is the added damping coefficient caused by the fluid; m_{ad} is the added mass caused by the fluid; and k_{ad} is the added stiffness coefficient caused by the fluid. Thus, the spring–dashpot is applied to present the interaction forces between the molten salt and graphite to reduce excessive demands on available computational resources.

3 Structural details and finite element model

3.1 TMSR graphite core

The design of the TMSR graphite core is shown in Fig. 2. Graphite serves as an internal structural material as well as a moderator in the TMSR. A large number of graphite bricks are involved in the TMSR core, forming reflectors. The reflectors, which consist of a top, side, and bottom reflector, together with the core support structure, form an inner space for fuel elements and at the same time serve as a flow guidance structure for the molten salt.

3.2 3D finite element model

A single-layer side reflector model of the TMSR core is shown in Fig. 3. The single-layer model is a typical unit of the side reflector core structure of the TMSR reactor, in which the dynamic response of an individual component and the interaction between bricks can be investigated. The model is composed of 16 graphite bricks, 16 keys and a plate. The bricks are all horizontally constrained by dowels on the plate. Each brick is interconnected with a key to

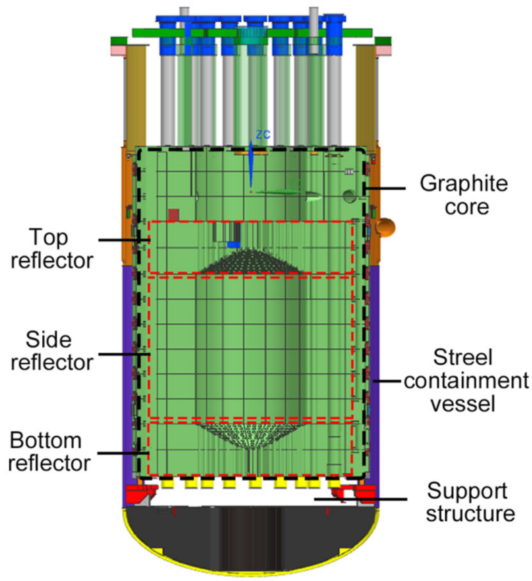

Fig. 2 (Color online) TMSR graphite core

restrain the circumferential relative motion. The whole model is mounted on a plate that generates the dynamic motion.

As a simplification, a 3D finite element model without side metallic component support, which is part of the TMSR side reflector structure, was developed using the ABAQUS 2016 software according to the parameters of the TMSR. The main parameters of the graphite material are listed in Table 1. To improve the accuracy of the model, the mesh on the corner and channel designs was refined as shown in Fig. 3. Some descriptions regarding this model are shown in Table 2.

Table 1 Material properties of graphite

Parameters	Values
Density (g/cm^3)	1.85
Young's modulus (GPa)	10
Poisson's ratio	0.21
Compressive strength (MPa)	85.3
Tensile strength (MPa)	41.5

Table 2 Description of the model

	Description
Components	16 bricks (173,312 elements)
	16 keys (16,560 elements)
	1 plate (50,624 elements)
Type of element	C3D8R[a]
Contact	All with self
Procedure	Dynamic, explicit
Output	Whole model
Time	20 periods of every job

[a]The C3D8R element is 3D 8-node element, with reduced integration (one integration point)

3.3 Boundary conditions

In this study, the aim was to investigate the dynamic behavior and response characteristics of the integrated graphite components. The seismic excitation applied on this model included the following: (case a) the excitation amplitude was from 3 to 20 mm in the *X* direction; (case b) the frequency ranges were from 2 to 10 Hz. During TMSR operation, the dimension of the graphite bricks will change

Fig. 3 (Color online) 3D modeling and detailed mesh of a single-layer graphite core

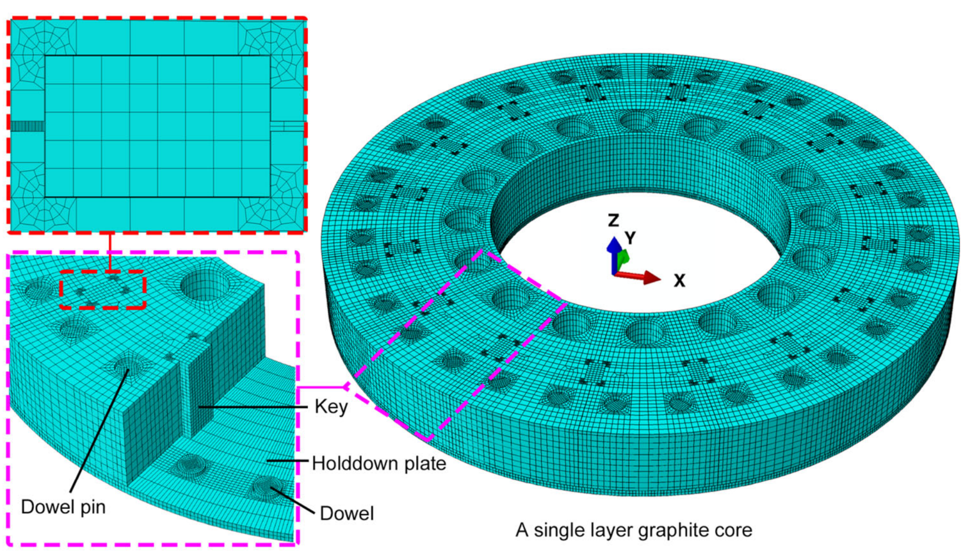

under high temperature and fast neutron irradiation [17, 18]. When the bricks contract, the gaps between the graphite bricks will increase, which will affect the dynamic response of the whole core structure. Consequently, the following cases were considered in the analyses: (case c) the gap between the dowel and brick, (case d) the gap between the key and keyway and (case e) the bypass flow gap between the two bricks. Another crucial factor that also needed to be considered was the effect of the molten salt in the TMSR (case f). All load and condition details are listed in Table 3.

3.4 Mesh sensitivity study

It is well known that the accuracy of numerical results is strongly dependent on the mesh density used. Better results would have been obtained by increasing the total number of elements, but the computational time and required computer memory would increase substantially as well. The 3D model with full degrees-of-freedom requires larger computational power and memory. Because of the limitations of the computer and software, it was impossible to use the largest mesh density in the analyses. Thus, an acceptable mesh density needed to be identified. Based on the numerical results, the peak maximal principal stress error of the total element numbers 140 K, 240 K and 340 K (as shown in Fig. 4) are 28.84 and 108.48% at 0.5 s, 8.42 and 128.14% at 1.0 s, and 7.05 and 149.17% at 1.5 s. The errors in the peak maximal principal stress of different mesh numbers are shown in Table 4. Therefore, the total number of elements of 240 K was used for all the analyses in this study.

4 Results and discussion

4.1 Brick maximal principal stress location

The graphite bricks were numbered from 01 to 16 in an anticlockwise direction with the 01 brick at 0 degrees (+ *Y* axis) as shown in Fig. 5a. The motion of the plate was assumed to be a sine wave with a forcing frequency 10 Hz

Table 3 Contents of numerical analyses

Cases	Values
(a) Different input amplitude (mm)	3, 5, 10, 15, 20
(b) Different input frequency (Hz)	2, 4, 6, 8, 10
(c) Gap between dowel and brick (mm)	0.5, 1, 1.5, 2
(d) Gap between key and keyway (mm)	0.5, 1, 1.5, 3
(e) Gap between two bricks (mm)	0.5, 1, 3, 5
(f) Effect of molten salt	–

and an amplitude of excitation of 5 mm. The maximal principal stress of the brick and its location were recorded as shown in Fig. 5b. It can be seen from the results that the location of the maximal principal stress always appears on 01, 08, 09 and 16. Compared to all the maximal principal stresses during the analysis process, the peak maximal principal stress (10.78 MPa) appears on number 08. Thus, further research objectives should be concentrated on the Number 08 brick.

4.2 Effect of excitation

4.2.1 Different amplitude

The displacements of the graphite bricks may affect the insertion of the control rods and shutdown material and consequently the reactor's shut down. Therefore, it is of vital importance, from the viewpoint of seismic design, to investigate the effect of different amplitudes of excitation. The vibration was excited by a sinusoidal wave whose frequency was a fixed value in the *X* direction. The value of the amplitude was a variable parameter. It was set to be 3 mm, 5 mm, 10 mm, 15 mm and 20 mm respectively. Different amplitude time histories of brick: 08-point P in the *Z* direction were recorded as shown in Fig. 6. The obtained results indicated that the displacement of the point in the *Z* direction during a certain frequency was sensitive to the oscillation amplitude, and collapse of the layer occurred when the excitation amplitude was greater than 10 mm. As shown in Fig. 6, the largest amplitude of the total structure of the graphite core is less than 10 mm, which has the smallest peak displacement response as compared to the other amplitude situations. These load and boundary conditions are extremely conservative compared to the actual seismic motion. For the graphite core, side metallic component support was ignored, which reduced the total dynamic response of the model. Therefore, such a collapse is not expected in the following seismic experiments and in the actual reactor core.

According to the figure, the whole single-layer model maintained its basic integrity and no graphite bricks were found to lose their initial position when the excitations were 3 and 5 mm. The No. 08 brick time histories of a maximal principal stress of 3 and 5 mm were recorded as shown in Fig. 7. It is clearly observed that the greater the excitation amplitude, the greater the maximal principal stress in brick No. 08. This result means the maximal principal stress also has a strong relationship with excitation amplitude.

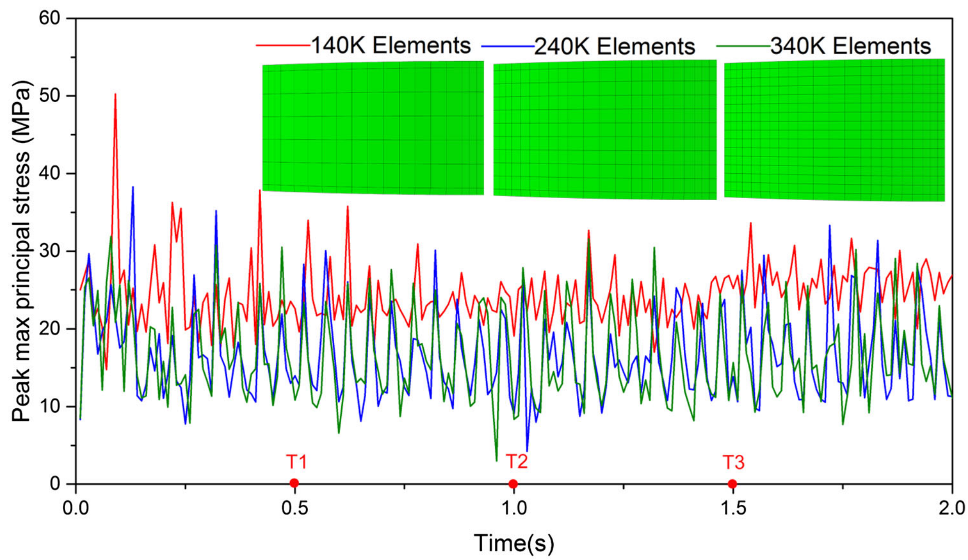

Fig. 4 (Color online) Peak maximal principal stress of different element numbers

Table 4 Errors of different mesh numbers

	Total element number (K)	Peak maximal principal stress of model		
		T1 (%)	T2 (%)	T3 (%)
Error (%)	140	108.48	128.14	149.17
	240	28.84	8.42	7.05
	340	–	–	–

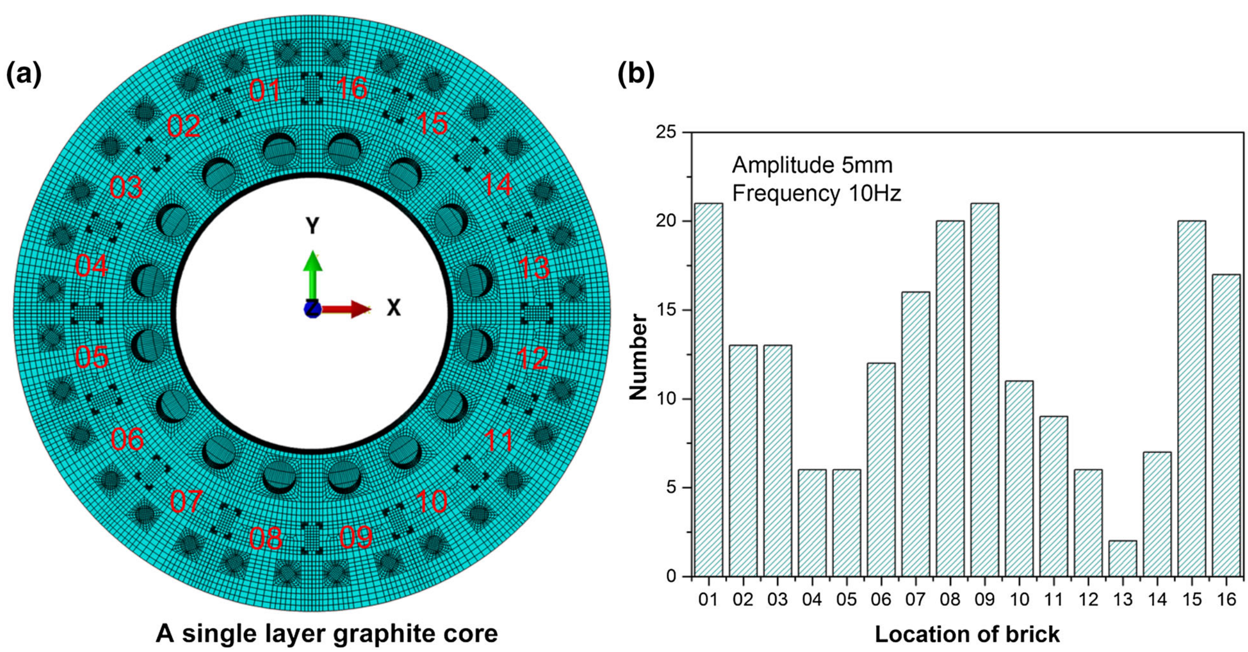

Fig. 5 (Color online) Brick maximal principal stress location

4.2.2 *Different frequencies*

The excitation frequency also has a significant influence on the dynamic analysis results. Thus, the effect of different values of frequency was investigated as described in this section. The frequency of an earthquake is usually less than 10 Hz; thus, five different excitation frequencies (2 Hz, 4 Hz, 6 Hz, 8 Hz and 10 Hz) on the dynamic

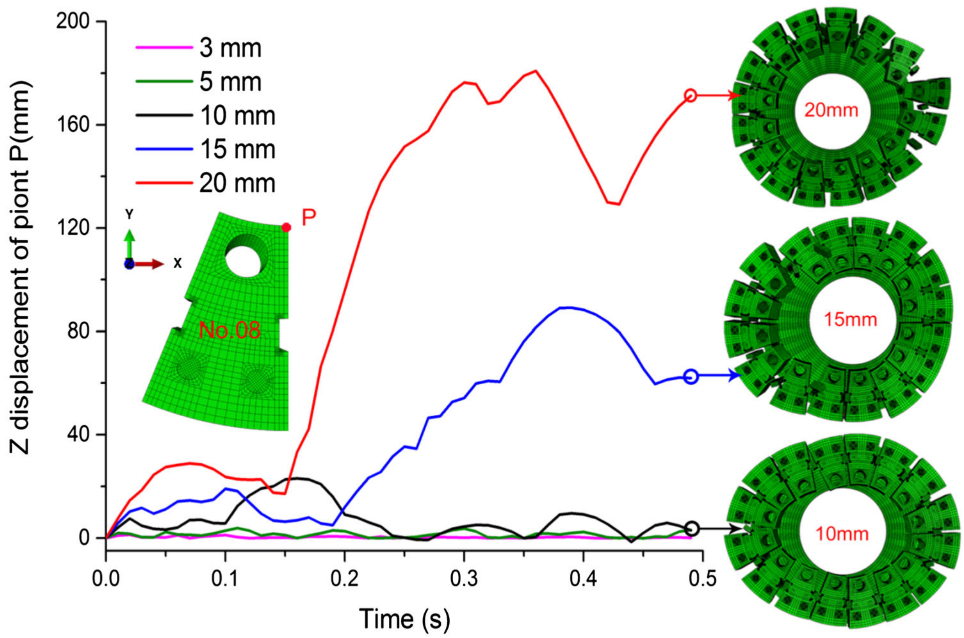

Fig. 6 (Color online) Time history of different amplitudes at point P

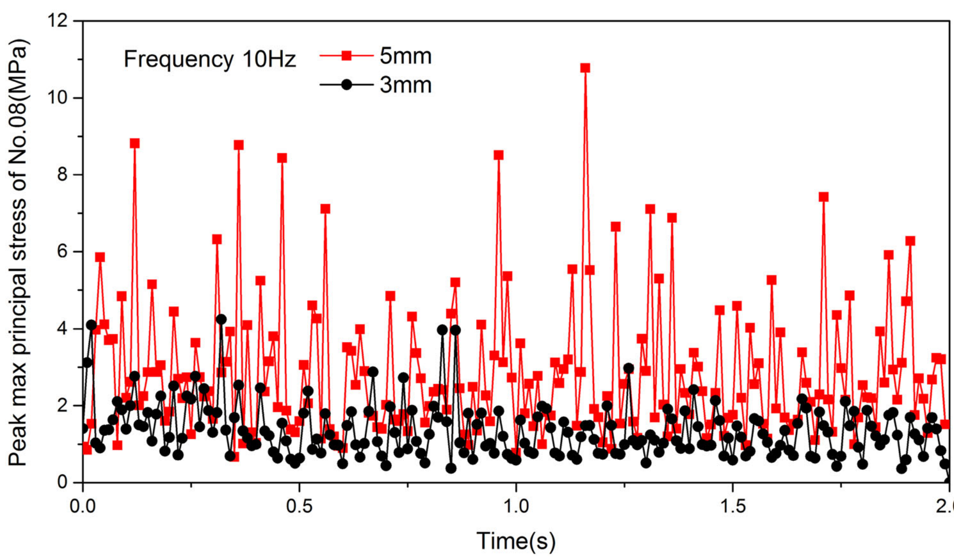

Fig. 7 (Color online) No. 08 brick peak maximal principal stress at 3 and 5 mm of amplitude

responses of the model are represented in Fig. 8. It is observed from the figure that the greater the excitation frequency, the greater the value of the maximal principal stress in brick No. 08 and the gap between No. 08 and the whole model bricks increases as the excitation frequency increases. In summary, the dynamic response of the model has a significant relationship with the excitation frequency.

4.3 Effect of design parameters

During TMSR operation, the dimensions of the graphite bricks will change under fast neutron irradiation. The graphite material will contract then turn around and return to the zero point, which is considered as the life end of the components. When the bricks contract, the gap between brick and dowel, the gap between the key and keyway and the bypass flow gap between two bricks will increase, which will affect the dynamic response of the whole core structure.

4.3.1 Gap between key and brick

The graphite brick nonlinear dynamic response is mainly caused by the interaction between the bricks and dowel. Different values of dowel diameter, namely the gap between the dowel and brick, are a vital factor. It was set to be 0.5 mm, 1 mm, 1.5 mm and 2 mm respectively in this section. The motion of the plate was assumed to be a sine

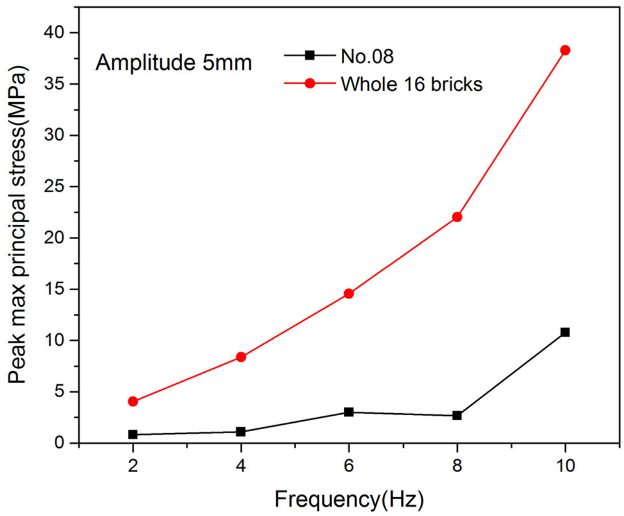

Fig. 8 (Color online) Peak maximal principal stress of different frequencies

wave with a forcing frequency of 10 Hz and an amplitude of excitation of 5 mm. The maximal principal stress of No. 08 and the maximal displacement of point P in the *X* direction were recorded as shown in Fig. 9. As is shown, the larger the gap between dowel and brick, the greater the maximal principal stress and absolute displacement of P. The reason for this phenomenon is because the gap affects the displacement of the brick, which makes the impact forces between the graphite bricks increase. Consequently, the gap should be as small as possible to reduce the collision between two bricks to ensure the structural integrity of the core.

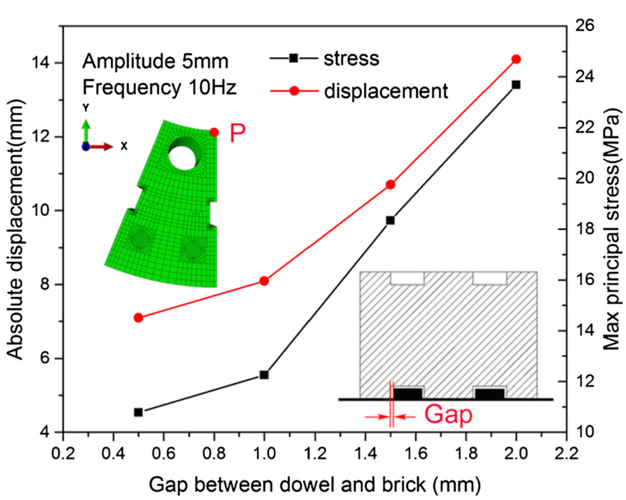

Fig. 9 (Color online) Peak maximal principal stress of brick No. 8 and displacement of P

4.3.2 *Gap between the key and keyway*

The whole graphite core consists of a large number of graphite components interconnected by keys. Keys are employed to restrain the circumferential relative motion to maintain the integrity of the graphite core. Thus, the gap between the key and keyway is also a vital factor in dynamic analysis. The plate was excited by a sinusoidal wave at a frequency of 10 Hz and an amplitude of 5 mm. The gap between the key and keyway was a study parameter. It was set at 0.5 mm, 1 mm, 1.5 mm and 3 mm. The key under consideration was that between brick: 08 and brick: 09. The maximal principal stress and absolute displacement in the *X*, *Y* and *Z* directions were recorded as shown in Fig. 10. It can be seen from Fig. 10 that the peak maximal displacement in the *X*, *Y* and *Z* directions at P increases along with the gap between the key and keyway and the maximal principal stress of key also showed this trend. The reason for these phenomena may be because the larger gap provides more room for the displacement of the key, which means there is less restraint on the key and the impact forces between the graphite brick and key increase.

We also found that the displacement in the *Z* direction increased rapidly compared to that of the *X* and *Y* directions. This was because the movement of the brick in the *X* and *Y* directions was not only confined by the gap between the key and keyway, but also the gap between the two bricks. When the gap between the key and keyway was 3 mm, the 1-mm gap between the two bricks had less of an effect on movement of the key. In the *Z* direction, the larger gap confined movement of the key less. Thus, the displacement in the *Z* direction increased rapidly.

4.3.3 *Bypass flow gap*

In this section, four different gaps were considered and compared to each other to obtain the dynamic response considering the gap effect between the two bricks. The plate was excited by a sinusoidal wave at a frequency of 10 Hz and amplitude of 5 mm. The gap between the two bricks was a study parameter. It was set to be 0.5 mm, 1 mm, 3 mm and 5 mm, respectively. The maximal principal stress and displacement in the *X*, *Y* and *Z* directions of P were recorded as shown as Fig. 11. The results showed that the gap between the two bricks had little influence on the displacement of point P in the three directions. The responsible factor for the slight variation in the displacement response at different gaps may be that the movement of the brick was also restricted by the gaps between the key and keyway. As previously discussed, the movement of the brick was confined not only by the bypass flow gap but also the gap between the key and keyway. The gap between the key and keyway was 0.5 mm in this section. When the

Fig. 10 (Color online) Peak maximal principal stress of key (between bricks Nos .08 and 09) and displacement of point P

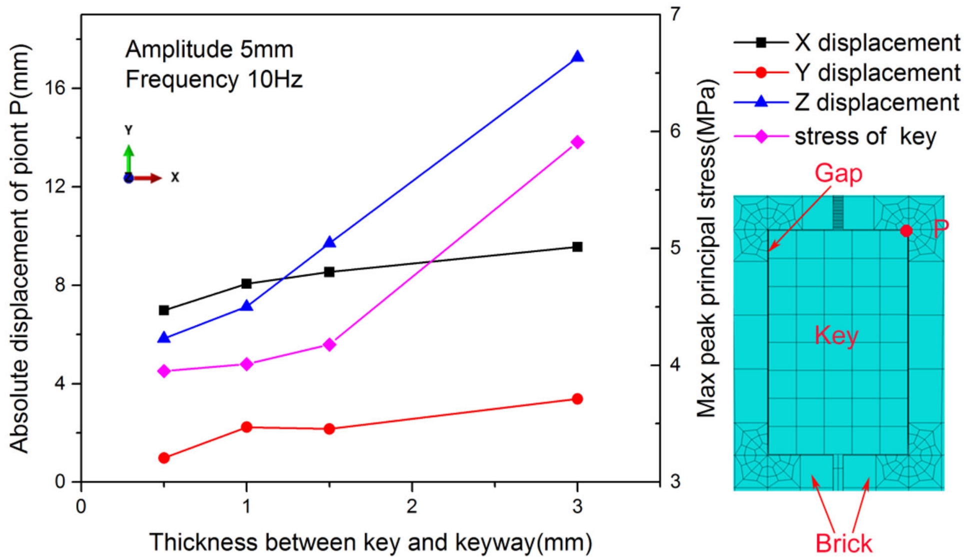

Fig. 11 (Color online) Peak maximal principal stress of brick No. 08 and displacement of P

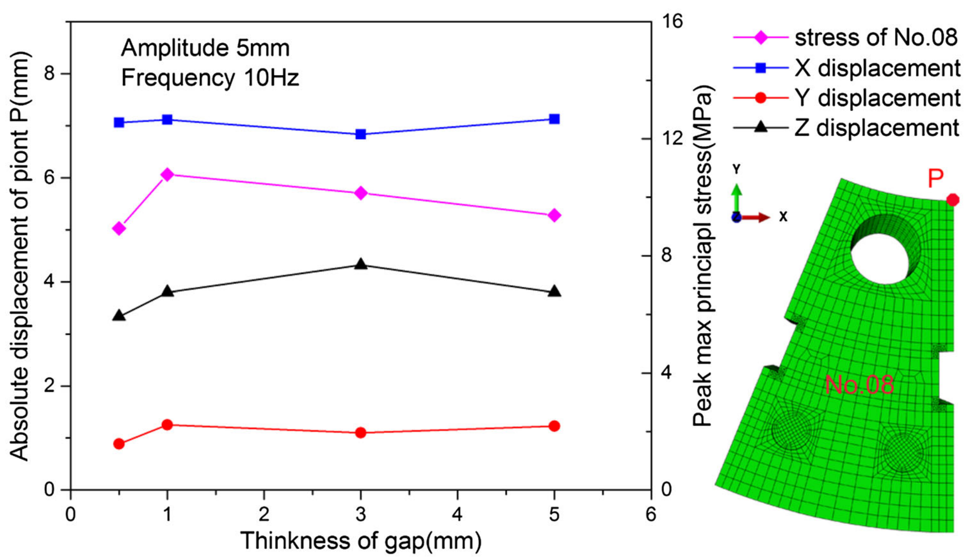

bypass flow gap was larger than 0.5 mm, the movement of the brick was restrained by the gap between the key and keyway. As for the peak maximal principal stress of brick: 08, the movement of the brick had strong a relationship with the stress. The bypass flow gap had little influence on the movement of the brick. Thus, the peak maximal principal stress also changed slightly.

Table 5 Stiffness and damping coefficient of different gaps

Groups (mm)	Added mass (kg)	Added damping	Stiffness (N/m)
3	9.76	833.40	39,492
5	8.41	755.59	37,776
10	6.65	540.25	32,140
15	4.87	455.38	29,839
20	4.51	432.80	29,147

4.4 Effect of molten salt

When a structural component is subjected to dynamic motion, the viscous fluid produces reaction forces that are generally referred to as added mass and added damping forces [19–21]. The added mass is associated with a mass of fluid that is accelerated by the structure and added damping is related to the shape of the structure and the viscosity of the fluid [22]. All the graphite components with a narrow gap between them are immersed in a TMSR and its mass density is much greater than that of gas coolant as in gas-cooled reactors. Therefore, the FSI

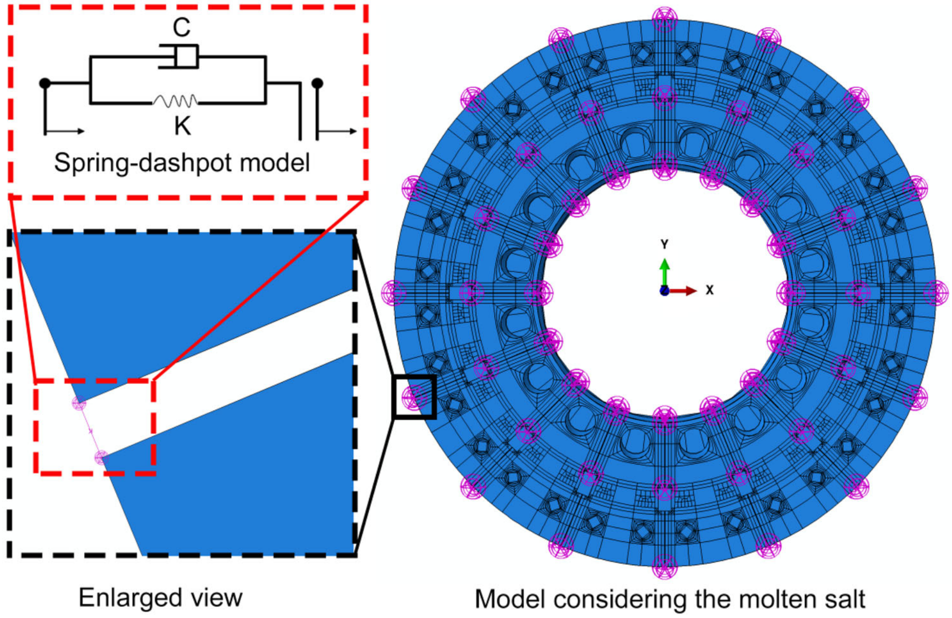

Fig. 12 (Color online) Simplification of the effect of molten salt

Table 6 Displacement of point P and peak maximal principal stress of No. 08 in air and liquid

	Air	Liquid
X (mm)	7.12	6.80
Y (mm)	1.25	1.05
Z (mm)	3.80	4.00
Max peak stress (MPa)	10.14	9.607

between the molten salt and graphite components cannot be ignored when subjected to an excitation load.

To reduce excessive demands on computational resources, such as computational time and computer physical memory, the spring–dashpot method was applied to represent the interaction forces between the molten salt and graphite bricks [8]. The dynamic characteristics of added mass, added damping and stiffness can be obtained by fitting the time history of vibration experiments with the analytical solution. Thus, the proper stiffness of the spring and the damping coefficient in the equivalent model can be obtained as shown in Table 5 [23]. Then, the equivalent model can be used in the seismic analysis of the TMSR graphite core as shown as Fig. 12. The vibration was excited by a sinusoidal wave at a frequency of 10 Hz and an amplitude of 5 mm in this section. The results of the displacement of point P in the three directions (*X*, *Y* and *Z*) and the peak maximal principal stress were recorded around brick:08 as shown in Table 6. As indicated, the existence of molten salt can reduce the peak maximum principal stress of brick: 08. In addition, the displacement of *X* and *Y* at point P is different from that of *Z*. The peak maximal displacement of P in the *X* and *Y* directions increased when the effect of molten salt was added, but the peak maximal displacement in the *Z* direction decreased considering the effect of the liquid. The phenomenon of the response of the graphite considering the FSI effects as concluded using the spring–dashpot model is that it only acts in the *X* and *Y* directions when the structure is subjected to excitation. In the horizontal *Y* direction, there is no restriction and the there is a stronger effect in the *X* and *Y* directions making movement of the brick more possible. Thus, the larger bypass flow gap is the best choice for a design reducing the dynamic behavior under earthquake loading. This is because there is more molten salt in this gap, thus there is a stronger damping effect for a dynamic response of graphite bricks and maintain the integrity of the graphite core.

5 Conclusions

A single-layer model was built based on a TMSR graphite core structure side reflector using commercial software ABAQUS 2016. The overall objectives of the present study were to numerically investigate the dynamic response and determine the seismic response of the graphite core. The dynamic responses under different excitations were obtained. Some conclusions can be drawn based on the numerical results of the maximal principal stress and displacement:

1. The location of the maximal principal stress always appears on bricks 01, 08, 09 and 16 when subjected to excitation in the *X* direction.
2. The whole single-layer model cannot maintain its basic structural integrity when the excitation amplitude is greater than 10 mm without side metallic component support and the maximal principal stress on brick No. 08 increases with an increase in amplitude and excitation frequency.
3. The movement of a brick is restrained by two factors namely the bypass flow gap and the gap between the key and keyway. For a certain gap of key and keyway, the bypass flow gap has a slight influence on displacement in the three directions and the maximal principal stress.
4. The effect of molten salt can reduce the peak maximal principal stress, thus a larger bypass flow gap is beneficial to maintain the integrity of the graphite core under earthquake loading.

References

1. J. Serp, M. Allibert, O. Beneš et al., The molten salt reactor (MSR) in generation IV: overview and perspectives. Proc. Nucl. Energy **77**, 308–319 (2014). https://doi.org/10.1016/j.pnucene.2014.02.014
2. Z. Dai, Thorium molten salt reactor nuclear energy system (TMSR). Molten Salt React. Thorium Energy (2017). https://doi.org/10.1016/b978-0-08-101126-3.00017-8
3. L. Sun, L. Shi, H.G. Wan et al., Seismic study on double-layer model of HTR graphite core structure. At. Energy Sci. Technol. **46**, 839–844 (2012). https://doi.org/10.1115/icone20-power2012-54961
4. W. Laframboise, T. Desmond, Nonlinear seismic analysis of a graphite reactor core. Nucl. Eng. Des. **110**, 131–146 (1988). https://doi.org/10.1016/0029-5493(88)90013-1
5. Stations NPG, IEEE recommended practice for seismic qualification of class 1E equipment for nuclear power generating stations. https://doi.org/10.1109/ieeestd.2005.96099
6. J. Merson, J. Bennett, *Computer Method for Analyzing HTGR Core Block Response to Seismic Excitation* (Los Alamos Scientific Lab., Los Alamos, 1976). https://doi.org/10.2172/7334839
7. T. Ikushima, T. Honma, Simplified Analytical Model for HTGR Core Seismic Response. J. Nucl. Sci. Technol. **16**, 605–612 (1979). https://doi.org/10.1080/18811248.1979.9730952
8. C. Zeng, H. Wang, A Three-Dimensional Rigid-Body Model for Seismic Analysis of the Pebble-Bed HTR Graphite Core Structure. Publisher (2013). https://doi.org/10.1115/icone21-15896
9. N. Tsuji, K. Ohashi, Development of seismic analysis model for HTGR core on commercial FEM code. ICONE (2015). https://doi.org/10.1299/jsmeicone.2015.23._icone23-1_105
10. K. Ahmed, J. Parker, D. Proffitt, Seismic response of the advanced gas cooled reactor core. Nucl. Eng. Des. **94**, 67–92 (1986). https://doi.org/10.1016/0029-5493(86)90154-8
11. K. Ahmed, The dynamic response of multi-layers AGR core brick arrays. Nucl. Eng. Des. **104**, 1–66 (1987). https://doi.org/10.1016/0029-5493(87)90303-7
12. K. Ahmed, S. Stojko, The non-linear seismic response of AGR core graphite brick slices correlation of experimental and analytical results. Earthq. Eng. Struct. Dyn. **15**, 159–188 (1987). https://doi.org/10.1002/eqe.4290150203
13. W. Rust, *Non-linear Finite Element Analysis in Structural Mechanics* (Springer, Berlin, 2016). https://doi.org/10.1007/978-3-319-13380-5
14. ABAQUS 2016 Documentation. Dassault Systemes Simulia Corporation. 2016. http://abaqus.software.polimi.it/v2016/books/hhp/default.htm?startat=pt02ch02s02.html
15. L. Lu, Y.R. Yang, P. Li et al., Added mass, added stiffness and added damping coefficients for a parallel plate-type structure. Appl. Mech. Mater. (2011). https://doi.org/10.4028/www.scientific.net/AMM.66-68.1738
16. L. Sargentini, B. Cariteau, M. Angelucci, Experimental and numerical analysis for fluid–structure interaction for an enclosed hexagonal assembly. AMSE (2014). https://doi.org/10.1115/pvp2014-28053
17. R. Nightingale, Radiation effects in graphite. Nucl. Sci. Eng. **26**, 286–287 (1966). https://doi.org/10.2172/4785225
18. D.K.L. Tsang, B. Marsden, J. Vreeling et al., Analyses of a restrained growth graphite irradiation creep experiment. Nucl. Eng. Des. **238**, 3026–3030 (2008). https://doi.org/10.1016/j.nucengdes.2007.12.017
19. T. Belytschko, Fluid–structure interaction. Comput. Struct. **12**, 459–469 (1980). https://doi.org/10.1016/0045-7949(80)90121-2
20. J.A. Jendrzejczyk, Added mass and damping of a vibrating rod in confined viscous fluids. J. Appl. Mech. (1976). https://doi.org/10.1115/1.3423833
21. W.D. Wilson, Added mass and damping coefficients fora hexagonal cylinder. J. Fluid. Struct. **5**, 503–519 (1991). https://doi.org/10.1016/s0889-9746(05)80003-9
22. R. Fritz, The effect of liquids on the dynamic motions of immersed solids. J. Eng. Ind. **94**, 167–173 (1972). https://doi.org/10.1115/1.3428107
23. Y. Zhong, X. Yang, D. Ding et al., Dynamic characteristics identification of two graphite bricks in molten salt reactor considering fluid–structure interaction. Nucl. Eng. Des. **335**, 409–416 (2018). https://doi.org/10.1016/j.nucengdes.2018.06.015